remote sensing

MDPI

Article

Enhancing Landslide Susceptibility Mapping by Integrating Neighboring Information in Slope Units: A Spatial Logistic Regression

Leilei Li [1], Mingzhen Jia [1], Chong Xu [2,3], Yingying Tian [4], Siyuan Ma [4] and Jintao Yang [5,*]

[1] School of Earth Science and Technology, Zhengzhou University, Zhengzhou 450001, China; stonejdx@zzu.edu.cn (L.L.); jiamingzhen123@gs.zzu.edu.cn (M.J.)
[2] National Institute of Natural Hazards, Ministry of Emergency Management of China, Beijing 100085, China; xc11111111@126.com
[3] Key Laboratory of Compound and Chained Natural Hazards Dynamics, Ministry of Emergency Management of China, Beijing 100085, China
[4] Key Laboratory of Active Tectonics and Volcano, Institute of Geology, China Earthquake Administration, Beijing 100029, China; tianyingying@ies.ac.cn (Y.T.); masiyuan@ies.ac.cn (S.M.)
[5] College of Economics and Management, China Agricultural University, Beijing 100083, China
* Correspondence: yangjt@lreis.ac.cn

Abstract: Landslide susceptibility mapping (LSM) is a vital tool for proactive disaster mitigation. Although numerous studies utilize slope units (SUs) for LSM, the limited integration of adjacency information, including spatial autocorrelation, often reduces predictive accuracy. In this study, GRASS GIS was utilized to generate slope units, and a spatial logistic regression (SLR) model was developed to incorporate the adjacency information of the slope units to predict the landslide susceptibility. Then, the spatial stratification heterogeneity patterns of landslide susceptibility were analyzed using GeoDetector. The results showed that the SLR model achieved an area under the curve (AUC) of 0.89, a notable improvement of 0.26 compared to the traditional logistic regression (LR) model that does not incorporate adjacency information. This indicates that incorporating adjacency information effectively enhances LSM accuracy by mitigating spatial autocorrelation. Furthermore, lithology, PGV, and distance to the epicenter were identified as the primary factors contributing to the formation of the spatial stratification heterogeneity of landslide susceptibility. Among these, the interaction between lithology and PGV exhibits the strongest nonlinear enhancement. By integrating both mapping units and their adjacency information, this study provides a novel approach to improving the predictive accuracy of LSM. Moreover, by analyzing the driving factors of spatial stratification heterogeneity in landslide susceptibility maps, the study advances the practical utility of LSM for disaster management and mitigation.

Keywords: slope units; landslide susceptibility mapping; spatial logistic regression model; spatial stratification heterogeneity; GeoDetector

check for updates

Citation: Li, L.; Jia, M.; Xu, C.; Tian, Y.; Ma, S.; Yang, J. Enhancing Landslide Susceptibility Mapping by Integrating Neighboring Information in Slope Units: A Spatial Logistic Regression. *Remote Sens.* **2024**, *16*, 4475. https://doi.org/10.3390/rs16234475

Academic Editors: Federico Raspini, Chao Zhou and Kunlong Yin

Received: 28 October 2024
Revised: 21 November 2024
Accepted: 26 November 2024
Published: 28 November 2024

Copyright: © 2024 by the authors. Licensee MDPI, Basel, Switzerland. This article is an open access article distributed under the terms and conditions of the Creative Commons Attribution (CC BY) license (https://creativecommons.org/licenses/by/4.0/).

1. Introduction

Landslides are the most common type of natural disaster [1,2]. Rainfall, earthquakes, water level changes, rapid snowmelt, volcanic eruptions and human activities are all trigger factors of landslides [3]. In mountainous areas, earthquakes are the main trigger factor for landslides [4]. Co-seismic landslides, as one of the secondary effects of earthquakes, frequently cause significant disasters [1,5,6]. The Wenchuan earthquake in China in 2008 triggered a large number of landslides, and nearly a quarter of the casualties were caused by the landslides [7,8]. Landslide Susceptibility Mapping (LSM) has demonstrated a strong predictive capability for potential landslide occurrences, facilitating the optimization of regional planning and construction prior to the onset of disasters [9]. However, the prediction accuracy of LSM is often influenced by the choice of mapping unit and the

adaptability of the employed model [10,11]. Thus, integrating these factors is essential for generating more accurate landslide susceptibility maps.

Mapping units are fundamental to LSM, with two primary types being raster units (RUs) and slope units (SUs) [12]. RUs are commonly used due to their ease of acquisition and mapping [13]. Nonetheless, the predictive accuracy of RUs is highly dependent on resolution, and their correlation with the geological environment is relatively low [14,15]. In addition, if the elevation value cannot be determined, even if a high resolution is used, the uncertainty will be higher than for a low resolution [16]. Landslides predominantly occur in mountainous regions, characterized by valleys and ridgelines, and RUs often fail to capture topographical continuity [17]. Conversely, SUs effectively address this limitation by aligning more closely with the actual landforms, and are thereby widely accepted for LSM [18–20]. In most studies, the extraction of SUs uses the curvature watershed method and the geomorphology method, which are based on the artificial extraction of valley ridgelines. However, it is difficult to obtain SUs by these two methods. Under these circumstances, the extraction of large-scale landslide units presents the challenges of being both time-consuming and prone to errors [21–23]. Therefore, the automatic zoning of slope units is particularly important. Under such circumstances, Alvioli et al. developed a modeling framework, r.slopeunits, which divides DEM data into large watersheds based on r.watershed of GRASS GIS, and then divides the watersheds into adjacent units according to the multiple flow strategy to obtain target slope units [24]. This software can be used to automatically extract SUs that are consistent with geomorphic characteristics [24]. There have been many studies that have used this software to make reasonable divisions of slope units and have obtained good results [25]. The consideration of neighboring information in the mapping of units is another critical factor for LSM, as landslides usually happen where they have occurred before and have strong spatial continuity [26]. Spatial autocorrelation, a common characteristic of spatial data, suggests that the neighboring units of landslide-prone areas also play an indicative role in landslide susceptibility. Given the inevitable impact of spatial autocorrelation on LSM modeling, recent studies have increasingly focused on optimizing models to mitigate this effect [27]. For instance, spatial residual models and spatial logistic regression models have been employed [28,29]. The spatial residual model typically requires the consideration of numerous factors; otherwise, it is prone to significant errors. However, it is impractical to encompass all the relevant factors within a single landslide susceptibility assessment [30,31]. The spatial logistic regression model incorporates the attribute information of neighboring mapping units as influencing variables for landslide occurrences, thereby accounting for spatial autocorrelation and significantly improving susceptibility mapping accuracy [13].

Post-mapping analysis of the spatial stratification heterogeneity of susceptibility maps offers critical insights for regional landslide disaster prevention and emergency management [32]. By examining the mechanisms of underlying past landslide events, we can effectively prevent and mitigate future landslides caused by earthquakes in the same area [33,34]. The spatial stratification heterogeneity in landslide distribution results from the interplay of multiple factors rather than a single cause. Hence, analyzing the interactions between these factors is crucial for practical slope engineering applications [35]. The GeoDetector tool proves to be an effective tool for identifying the drivers of spatial stratification heterogeneity in landslide susceptibility maps, as it considers both individual influencing factors and their interactions [36]. This approach is instrumental in validating and applying LSM, offering substantial information for engineering applications.

To enhance the accuracy of landslide susceptibility maps, this study advances LSM methods and applications through three main aspects: (a) generating slope units for LSM using GRASS GIS; (b) modeling LSM by incorporating the adjacency information of neighboring units through spatial logistic regression and making comparisons with the results of the logistic regression model; and (c) analyzing the influencing factors and their interactions to understand the mechanisms behind the spatial stratification heterogeneity of landslide susceptibility.

2. Study Area and Data

2.1. Study Area

In 2013, a magnitude 5.9 earthquake struck Minxian County, Dingxi City, Gansu Province, China [6]. This earthquake triggered numerous co-seismic landslides. The study area was delineated as an elliptical region along the seismic intensity contour, encompassing the epicenter. It spans approximately 34°25′–34°43′N latitude and 103°51′–104°16′E longitude, covering an area of 927.35 km^2 with an average slope of 24.19°. The region experiences a plateau continental climate, with an average annual temperature ranging from 5.0 to 7.0 °C. Elevations in the area vary between 2192 and 3360 m, reflecting its high-altitude terrain. Influenced by the interaction of continental air masses and subtropical warm, humid air masses, coupled with topographical effects on the atmospheric uplift, the region exhibits a cold and humid climate. The Tao River serves as the primary river flowing through the study area.

The channel area of the study region consists of Quaternary sandy deposits, with Late Cenozoic sandstones distributed along both sides of the channel and Early Permian quartz sandstones covering most of the area. In the southwest and southern regions, Devonian carbonaceous shale and silty shale are present, respectively [6]. The continuous uplift and compression of the Qinghai-Tibet Plateau result in strong tectonic movements and frequent seismic activity, shaping a complex landscape characterized by numerous valleys and steep mountains.

The study area is situated in the north-central section of the North–South Seismic Belt, a region highly susceptible to earthquakes due to the presence of numerous large-scale active fault zones [37]. Figure 1 provides a comparative overview of the landslide conditions in the study area before and after the seismic event. The seismogenic structure responsible for the earthquake is a branch fault on the northern side of the Lintan–Dangchang Fault Zone, which lies between the eastern Kunlun Fault Zone and the northern edge of the western Qinling Fault Zone. This fault zone features a southward thrust with a general NWW-NW strike, a NE dip, and a dip angle of 50–70°, combined with a left-lateral strike-slip component. Variations in fault zone activity characteristics contribute to post-earthquake disasters, such as landslides and collapses [20]. To enhance the accuracy of the statistical analysis of the co-seismic landslides, AI Earth was utilized to perform a comparative analysis of pre- and post-seismic remote sensing imagery. The pre-earthquake satellite imagery, dated 6 April 2013, is shown in Figure 1a, while the post-earthquake imagery, captured on 1 August 2013, is displayed in Figure 1b.

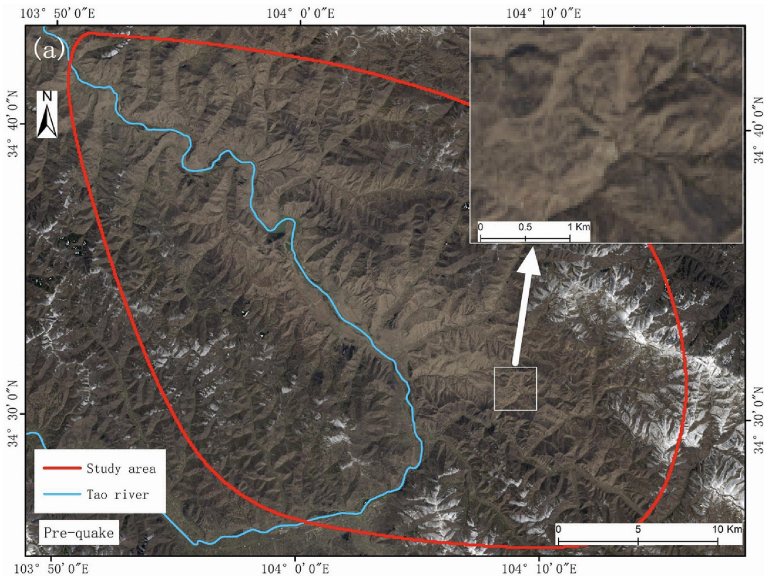


Figure 1. *Cont.*

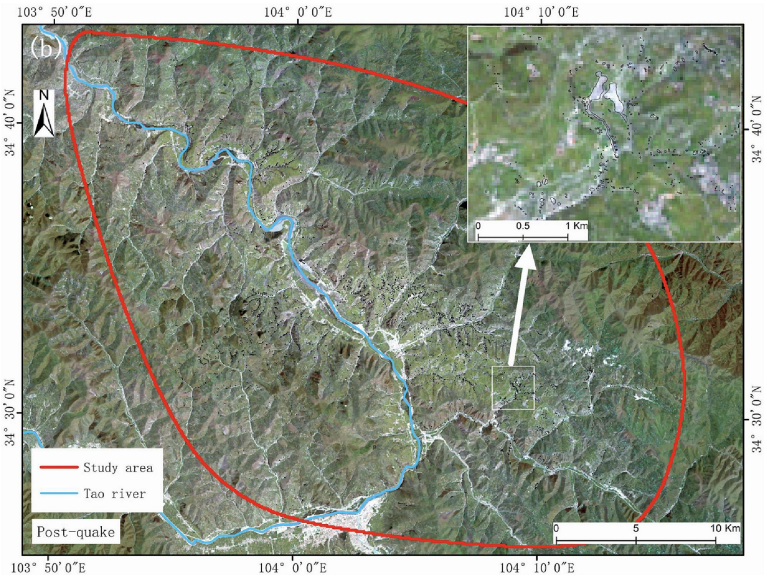


Figure 1. Maps showing the co-seismic landslides based on pre- and post-quake AI Earth images. (**a**) Pre-quake satellite image; (**b**) post-quake satellite image.

2.2. Data

Using high-resolution Google Earth images and comparing them with ZY-3 images, the landslide after the Minxian earthquake in 2013 was identified [37]. There are various types of landslides in the study area, such as falls, slides, and slumping on steep loess ridges, as well as deep continuous landslides and soil collapse [6]. In the study area, there are a total of 8526 landslides, with areas ranging from 3.68 to 51,246.19 m^2. Among them, 8236 landslides are less than 1000 m^2, accounting for 96.60% of the total number of landslides, while only 290 are large. Most of the landslides are soil landslides, with few rock landslides. These landslides are generally distributed along the Tao River, concentrated in the central and southern parts of the study area, where land use types are mostly cultivated land. The geographical location, topography, and distribution of landslides in the study area are illustrated in Figure 2.

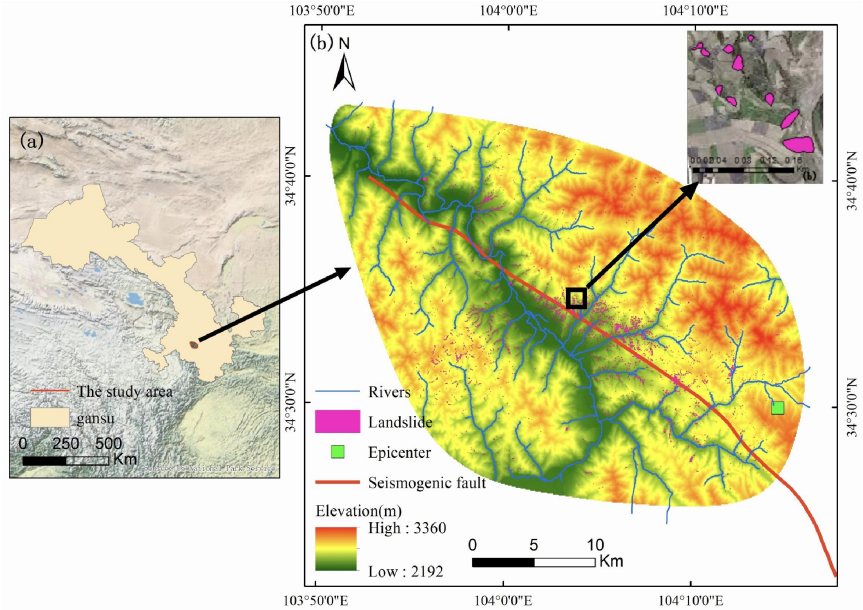


Figure 2. Inventory map of earthquake landslides in Min County earthquake epicenter area. (**a**) Location of the study area, (**b**) landslide inventory.

According to the geological conditions in the study area, eight factors were selected for LSM, including topographic and geological conditions (Figure 3). The topographic landform category includes four influencing factors: elevation, slope, profile curvature, and topographic wetness index (TWI). The elevation data have a resolution of 5 m and can be obtained from the AW3D website (https://www.aw3d.jp/en/ (accessed on 1 February 2014)) [38]. Slope, curvature, and TWI can be derived from the elevation data. The geological conditions include four influencing factors: distance to the epicenter, distance to the seismogenic fault, peak ground velocity (PGV), and lithology. The distance to the seismogenic fault and the epicenter represents the distance from the centroid of each unit to the seismogenic fault and the epicenter, respectively. Proximity to the seismogenic fault significantly increases both the probability and severity of landslides, while closer proximity to the epicenter is associated with a higher likelihood of landslide occurrence. PGV is an important indicator for describing earthquake intensity, and PGV data have a quantitative relationship with landslide density, according to the ShakeMap released by the United States Geological Survey (USGS) [39]. The lithology data come from the 1:200,000 geological map classified by stratigraphic age provided by the National Geological Data Center [6].

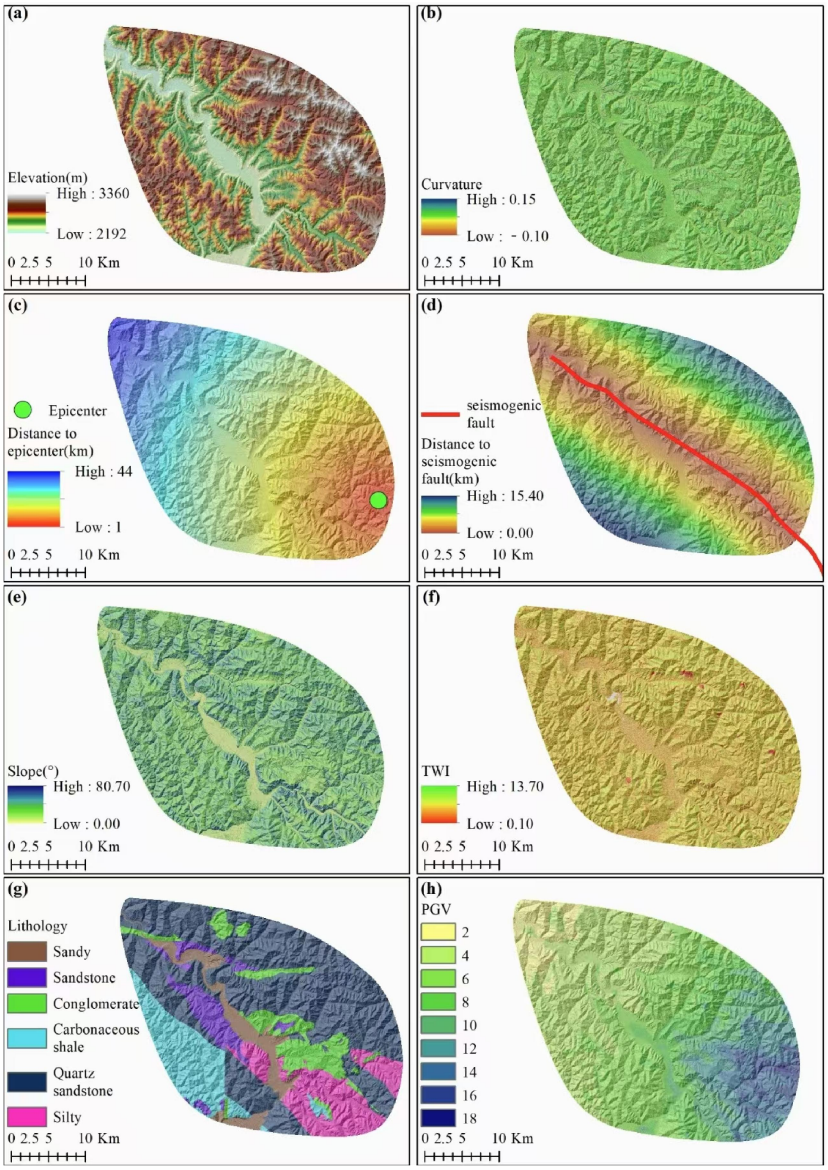


Figure 3. Maps showing distribution of influencing factors in study area. (**a**) Elevation; (**b**) curvature; (**c**) distance to epicenter; (**d**) distance to seismogenic fault; (**e**) slope; (**f**) TWI; (**g**) lithology; (**h**) PGV.

3. Method

This study evaluated landslide susceptibility by following three core steps: first, slope units were generated from elevation data using the GRASS GIS 7.8, and the attributes of each influencing factor were mapped to the slope units based on their spatial locations; second, an LR model and SLR model were employed to assess landslide susceptibility, and the results were verified and compared; and finally, the spatial stratification heterogeneity mechanisms in the landslide susceptibility map were analyzed using GeoDetector. Figure 4 depicts the comprehensive technical workflow of the study.

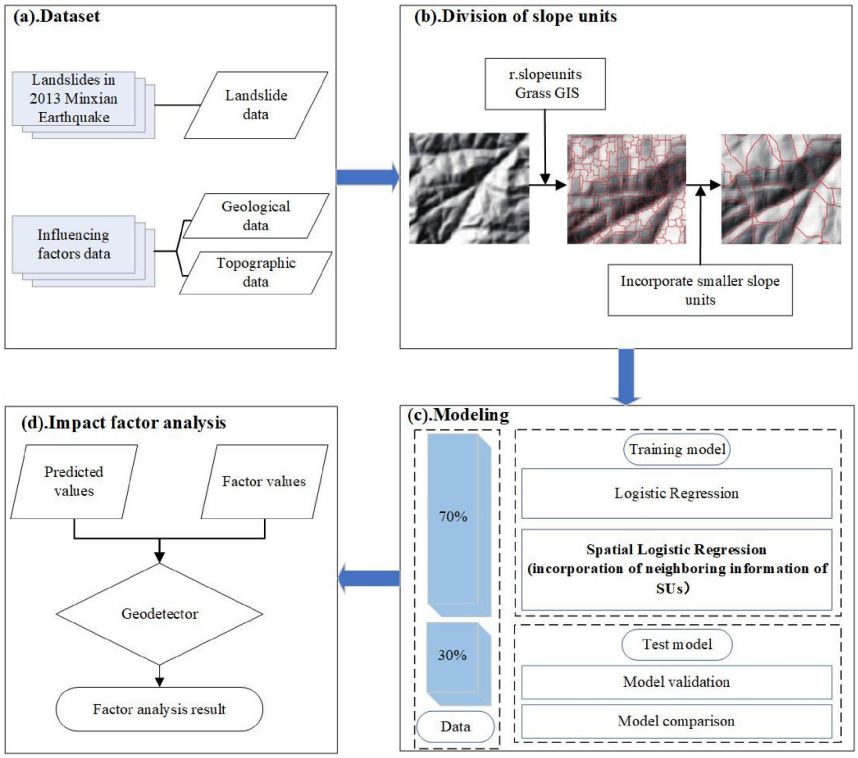


Figure 4. Workflow of the method proposed in this research to predict earthquake-induced landslide events.

3.1. Slope Unit Delineation

A slope unit (SU) refers to a topographic unit enclosed by drainage and watersheds. Several methods have been proposed for the division of slope units; among these, the r.slopeunits v1.0, based on GRASS GIS, is an automatic way to roughly divide the elevation data along the landform into SUs [40]. The parameters that need to be set include the following: the initial flow aggregation area threshold t (km^2); the reduction coefficient r, used to iteratively calculate the new value of the flow aggregation area threshold; the minimum square difference c of the terrain slope direction within a slope unit; and the minimum area a (m^2) of the SU [40]. Parameters a and c are important parameters for controlling the size of the SUs, and the time required by r.slopeunits to extract the SUs is also closely related to a and c [20].

Considering previous research and the actual shape size of the slope units in the study area, the following values were obtained, corresponding to several combinations of input parameters in the r.slopeunits software: t = 0.08 km^2, 0.1 km^2, 0.2 km^2, 0.3 km^2; a = 70,000 m^2, 90,000 m^2, 150,000 m^2; c = 0.15, 0.2; and r = 5. The slope morphology of t = 0.1 km^2, a = 70,000 m^2, c = 0.2, and r = 5 was the most consistent with that of the actual study area. To avoid excessive area differences between the slope elements, the slope units with too small an area were merged with adjacent units, and a total of 8647 SUs were

generated. These units have a maximum area of 0.76 km^2 and an average area of 0.11 km^2 (Figure 5). There were 6743 units without landslides and 1904 units with landslides.

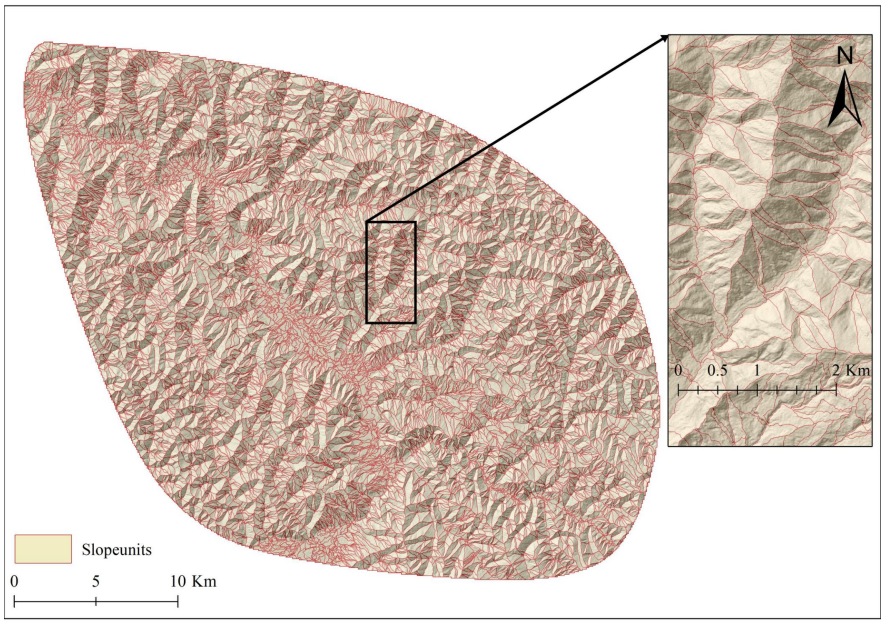


Figure 5. The slope unit map.

3.2. Spatial Logistic Regression Model

The logistic regression model can predict the probability of the landslide by using the linear regression relationship between the variables and multiple independent variables [19]. Since the variable that occurs in the landslide is a dual variable, the independent variable type can be continuous or discrete [41]. The equation is as follows:

$$Y = ln\frac{P(x)}{1-P(x)} = \beta_0 + \beta_1 X_1 + \beta_2 X_2 + ... + \beta_i X_i + \varepsilon \ (i = 1, 2, ..., n) \quad (1)$$

$$P = \frac{e^Y}{1+e^Y} \quad (2)$$

where X_1, X_2, ... X_i are independent variables, β_0 is the intercept coefficient, and β_1, β_2, ..., β_i are the undetermined regression coefficients corresponding to each factor. $P(x)$ is the probability of landslide occurrence, P is the prediction probability, and x is the conditional factor.

$$Y = ln\frac{P(x)}{1-P(x)} = \beta_0 + \beta_1 X_1 + \beta_2 X_2 + ... + \beta_i X_i + \rho WY + \varepsilon \ (i = 1, 2, ..., n) \quad (3)$$

In practical situations, the occurrence of landslides is not only related to various factors under the influence of the spatial autocorrelation effect, but also to the environment around the landslides [10]. Therefore, in addition to being influenced by the independent variable, the value of the Y variable also needs to consider the neighboring information of SUs. Spatial regression is a modification of the regression equation that incorporates the adjacency matrix [10]. Equation (3) represents the spatial autoregressive model, which considers the adjacency relationship of spatial data based on Equation (1) [27,42]. ρ is the coefficient of spatial autocorrelation of Y, ε is the error term that conforms to a normal distribution, W is the n-dimensional spatial adjacency matrix, and n is the total number of samples. Compared with Equation (1), the increase of ρWY in Equation (3) excludes the spatial

structure information contained in the adjacency relationship from the residuals, reducing the possibility of obtaining biased estimates. The specific content of W is as follows:

$$W = \begin{bmatrix} 0 & f(d_{12}) & \cdots & f(d_{1j}) \\ f(d_{21}) & 0 & \cdots & f(d_{2j}) \\ \vdots & \vdots & \ddots & \vdots \\ f(d_{i1}) & f(d_{i2}) & \cdots & 0 \end{bmatrix} \tag{4}$$

$$L = y\ln\frac{e^{(\alpha+X\beta+\rho Wy)}}{1+e^{(\alpha+X\beta+\rho Wy)}} - (1-y)\ln\left(1+e^{(\alpha+X\beta+\rho Wy)}\right) \tag{5}$$

Equation (4) represents the adjacency matrix, and it is used to represent the adjacency relations in a SU, especially in graph theory and network analysis. If two mapping units are adjacent, the value of $f(d_{ij})$ is 1; otherwise, if they are not adjacent, $f(d_{ij})$ is 0. Equation (5) is the maximum likelihood function, which is used to solve the bias caused by the traditional least squares method and other parameter estimations.

3.3. Implementation of SLR

The 8647 SUs obtained above were used as mapping units, and the mean values of the independent variables of six factors, including elevation, curvature, distance to the epicenter, distance to the seismogenic fault, slope, and TWI, were assigned to the SUs. For the two discrete factors, lithology and PGV, the value with the largest proportion of landslide area was assigned to the corresponding SU. Dependent variables need to be considered during SLR modeling. If there is a landslide in the slope unit, the value of Y is 1; otherwise, it is 0. The spatial logistic regression model, as a supervised learning model, relies on training data to estimate parameters, and requires test data to verify the generalization ability and performance of the model. This process ensures that the model can have a better prediction effect in practical application. Considering the difficulty of acquiring future data sets, in this study, we adopted the conventional random sampling method for verification; 70% of the samples were used for training and 30% for testing [43]. The LR model and SLR model were solved using the free R-INLA package [44,45], and the expression for the SLR model is as follows:

$$\begin{aligned} \mathrm{Y} = {} & (0.173 \times \text{Elevation}) + (-0.012 \times \text{Curvature}) + (-0.406 \times \text{Distance to epicenter}) \\ & + (-0.237 \times \text{Distance to seismogenic fault}) + (-0.040 \times \text{Slope}) + (0.017 \times \text{TWI}) \\ & + (-1.420 \times \text{Lithology(sandy)}) + (-1.174 \times \text{Lithology(sandstone)}) \\ & + (-1.509 \times \text{Lithology(conglomerate)}) + (-0.611 \times \text{Lithology(silty shale)}) \\ & + (-1.928 \times \text{Lithology(carbonaceous shale)}) + (-2.159 \times \text{Lithology(quartz sandstone)}) \\ & + (-1.425 \times \text{PGV (2)}) + (-1.164 \times \text{PGV (4)}) + (-1.197 \times \text{PGV (6)}) + (-1.353 \times \text{PGV (8)}) \\ & + (-1.443 \times \text{PGV (10)}) + (-1.153 \times \text{PGV (12)}) + (-1.781 \times \text{PGV (14)}) \\ & + (-1.207 \times \text{PGV (16)}) + (-0.274 \times \text{PGV (18)}) \end{aligned}$$

The regression coefficients represent the impact of influencing factors on landslide susceptibility and are determined by the dimensions of each factor. The regression coefficient of a categorical variable means the relative risk of each category. A negative regression coefficient indicates that the category is less likely to trigger the event compared to the reference category. For instance, in this study, the regression coefficient for quartz sandstone is −2.159, whereas for silty shale it is −0.611, suggesting that quartz sandstone has a lower likelihood of causing landslides compared to silty shale. The regression coefficient, therefore, reflects the relative risk. For continuous independent variables, the regression coefficient indicates the direction and magnitude of influence on the dependent variable. A positive coefficient implies that an increase in the independent variable raises the probability of landslide occurrence, whereas a negative coefficient indicates that the probability decreases as the independent variable increases.

3.4. GeoDetector

GeoDetector can identify the causes of spatial stratification heterogeneity in landslide susceptibility maps caused by influencing factors and their interactions [36]. This study used the free R package "GD" to process the data [35,46]. The predicted value of each slope unit was taken as the dependent variable Y, and the continuous variable X is categorized. The number of categories for each continuous variable was set to 6–10 categories. The "GD" package was used to determine the best classification method and classification number of each continuous factor. It calculates the contribution of each factor to landslides and their combined effect on landslides.

GeoDetector includes four parts: a risk detector, a factor detector, an ecological detector, and an interactive detector [47]. Among these, the factor detector and interactor detector are the most helpful for the impact factor analysis of this study. The role of the factor detector is to detect the spatial heterogeneity of Y and the extent to which variable X explains the spatial heterogeneity of attribute Y. The interactor detector is used to identify the interactions between variables X; that is, to assess whether two factors acting together increase or decrease the explanatory power of the dependent variable Y, or whether the effects of these factors on Y are independent [48]. The principle of GeoDetector is as follows:

$$q = 1 - \frac{1}{N\sigma^2}\sum_{i=1}^{m} N_i\sigma_i^2 \quad q \in [0,\ 1] \tag{6}$$

where m is the number of categories of the independent variable X—taking lithology as an example, m is 6; N is the total number of slope units; σ_i^2 is the variance of the i-th layer of the dependent variable Y; and σ^2 is the variance of the whole study area Y. The q value indicates the extent to which the independent variable X explains the spatial stratification heterogeneity of the dependent variable, and a higher q value indicates a greater contribution of X to the landslides.

4. Results

4.1. Model Verification and Comparison

The predictive accuracy of the model can be characterized by the receiver operating characteristic (ROC) curve and the area under the curve (AUC). The farther the ROC curve is from the diagonal, the better the differentiation of the model [49]. An AUC value between 0.7 and 0.9 indicates that the model has a high accuracy [38,50]. In addition to the AUC, the confusion matrix not only quantitatively assesses the predictive performance of the model, but also reveals more detailed information. In this study, the AUC of the LR and SLR models were 0.63 and 0.89, respectively (Figure 6). According to the confusion matrix of the two models in Table 1, the overall prediction accuracy of SLR was 85.20%, which was 17.70% higher than that of the LR model, and the recall also increased by 22.07%. The results show that the SLR model has a higher accuracy.

Table 1. The confusion matrix of LR and SLR.

Method	Landslide Occurred	Prediction		Recall	Accuracy
		Yes	No		
LR	Yes	353	218	61.82%	67.50%
	No	625	1398	69.10%	
SLR	Yes	479	92	83.89%	85.20%
	No	292	1731	85.57%	

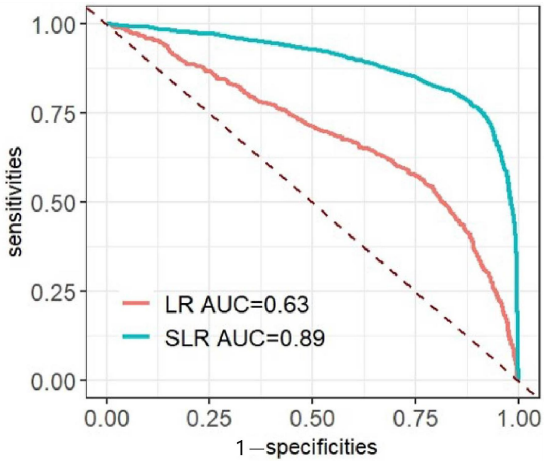


Figure 6. Comparison of the LR and SLR models by using the ROC curve. AUC is the acronym of the area under the ROC curve.

4.2. Landslide Susceptibility Map

The Seed Cell Area Index (SCAI) is an indicator for assessing the efficiency of classification, with lower SCAI values in highly sensitive areas and higher SCAI values in low-sensitive areas [51]. Table 2 shows that the SLR model has a gradually increasing sensitivity from high to low SCAI values, indicating that the classification results are reasonable, while the LR model has a large SCAI value in the high-risk area, indicating that the LR model overestimates the high-risk area. Figure 7 shows the spatial effect of the SUs' adjacent information extracted by the SLR model. The spatial effect indicates that SUs can effectively reduce the influence of spatial effects on the results. The predicted landslide risks are divided into three categories using the classification of natural break points [52]. The landslide susceptibility grade distribution maps obtained by the LR and SLR models are shown in Figure 8a and 8b, respectively. The LR model divides most areas into the same disaster level, while the SLR model is more dispersed.

Table 2. The densities of landslides among susceptibility classes of both methods.

Model	Sensitivity Level	Area Ratio	Number of Landslides	SCAI
LR	Low	46.36%	3998	1.003
	Moderate	34.21%	2990	0.989
	High	19.41%	1659	1.012
SLR	Low	50.93%	4385	1.004
	Moderate	35.13%	3041	0.999
	High	13.92%	1221	0.987

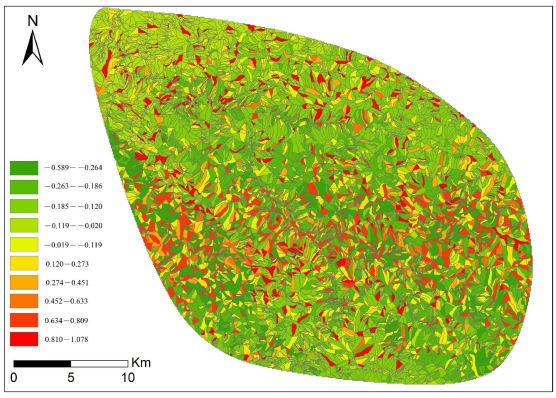


Figure 7. Map of the study area illustrating the neighboring structural effect.

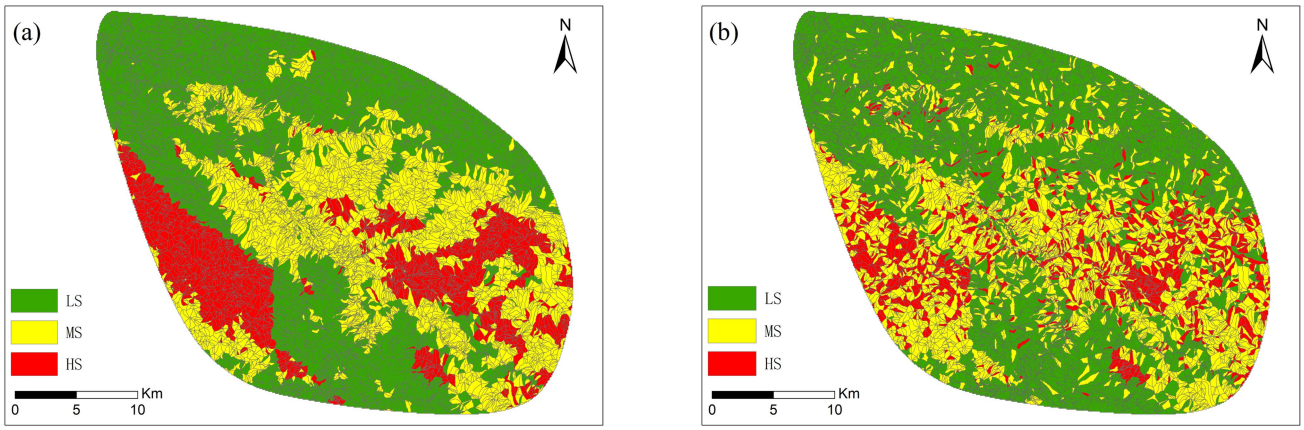


Figure 8. Landslide susceptibility map. (**a**) is the landslide susceptibility map produced by LR. (**b**) is the landslide susceptibility map produced by SLR. LS, MS, and HS, respectively, indicate three landslide susceptibility levels of low, moderate, and high.

4.3. Factor Analysis for the Spatial Pattern of the Landslide Susceptibility Map

The spatial stratification heterogeneity of the landslide susceptibility map was investigated using factor analysis. Lithology, PGV, and distance to the epicenter were identified as the three factors contributing most significantly to the spatial distribution of the landslides (Table 3), and their q values are 0.299, 0.207, and 0.175, respectively. This indicates that lithology alone can explain 29.9% of the spatial stratification heterogeneity of landslide susceptibility. This result shows that earthquakes are a trigger factor of landslides, but their main controlling factor is lithology. The interaction analysis of factors shows that, while the interactions between lithology and slope, distance to the epicenter, and PGV involve bivariate enhancement, the enhancement of other factors is nonlinear. Among these, the interaction between lithology and PGV shows the strongest nonlinear enhancement, followed by the interaction between lithology and distance to the epicenter (Figure 9). The risk detector reflects the average area of landslide occurrence in each layer of the impact factor, as well as the statistically significant difference in the average landslide area between the layers. DEM, curvature, distance from fault, slope, TWI, and PGV all show significant differences (Figure 10). Ecological detection was used to compare whether there were significant differences in the effects of the two factors on the spatial distribution of landslides. The results showed that all the factors have significant effects on landslides (Figure 11), indicating that the factors selected in this study are reasonable and there is no redundancy, which affects the accuracy of landslide susceptibility mapping [53].

Table 3. The factor detector calculated by Geodetector. (X1–X8 represent DEM, curvature, distance to epicenter, distance to fault, slope, TWI, lithology, and PGV, respectively).

Variables	X7	X8	X3	X1	X4	X5	X6	X2
q	0.299	0.207	0.175	0.030	0.016	0.013	0.002	0.001
p	<0.05	<0.05	<0.05	<0.05	<0.05	<0.05	<0.05	<0.05

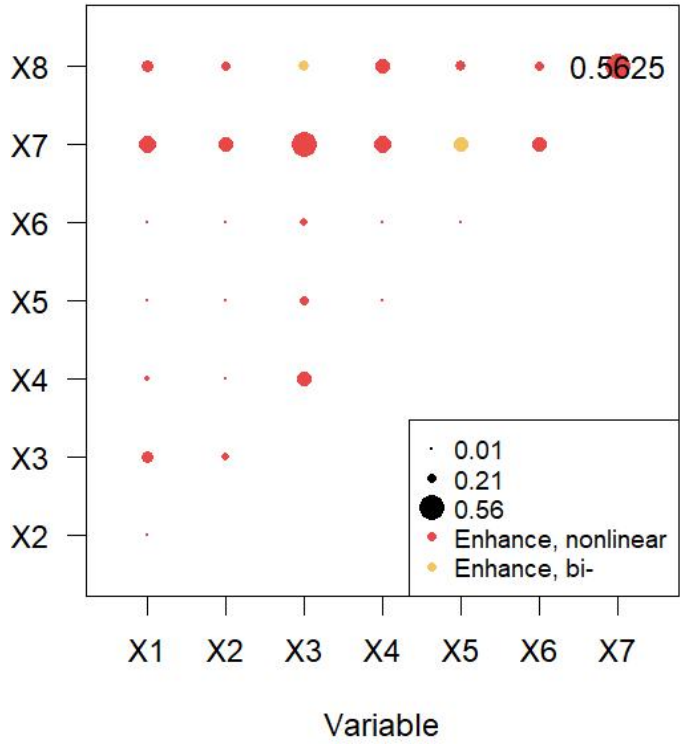


Figure 9. Interaction detector result.

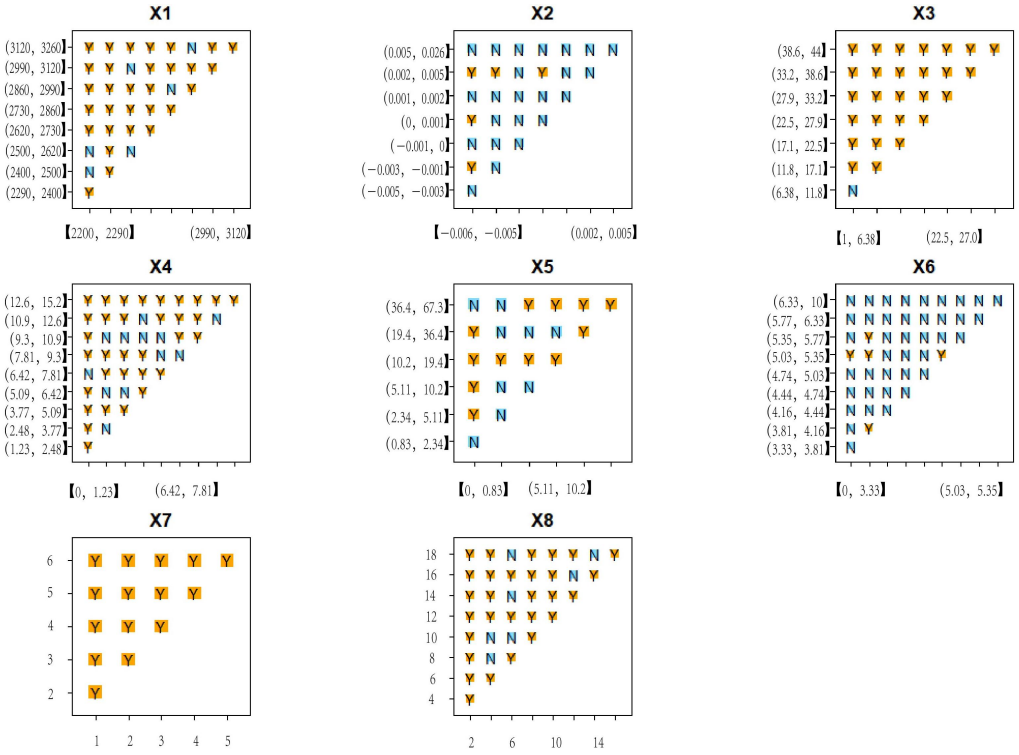


Figure 10. Risk detector result.

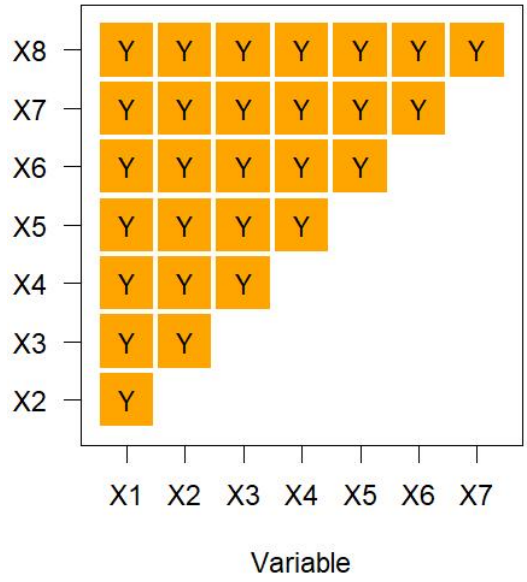


Figure 11. Ecological detector result.

5. Discussion

This study addressed the influence of the spatial autocorrelation of spatial data on LSM, by dividing slope units and including the neighboring information of SUs in susceptibility modeling. Additionally, by analyzing the contributions of the interactions among various factors to the spatial heterogeneity of landslide susceptibility, the accuracy of the susceptibility map was improved. Compared with the LR model, the AUC and confusion matrix of the SLR model had a higher accuracy, which indicated that the landslide susceptibility evaluation established by the SLR model was more consistent with the landslide occurrence rule compared with the LR model. The SLR model demonstrates objectivity, feasibility, and a strong predictive capability for the study area. This evaluation can play a certain guiding role in the prevention and management of landslide disasters in the region.

The use of SUs significantly reduces the spatial autocorrelation of landslide occurrence. The spatial effect map obtained by the SLR model is only approximately the same as the actual landslide density map (Figure 8b, while previous studies based on grid cells have shown that there is a strong correlation between the spatial effect map and the actual landslide density map [13]. This is mainly due to the consideration of the spatial similarity of adjacent units. RUs fail to consider the spatial similarity of adjacent units. SUs are extracted from RUs, and the value of each factor attribute in each SU is not particularly different, while the adjacent SUs show differences. In this study, 96% were small landslides, and one SU included many landslides, which greatly reduced the correlation of landslide occurrence among adjacent units, thereby making the spatial data more independent. For landslide susceptibility mapping, an increased independence on input data leads to reduced negative effects of spatial autocorrelation on the model. Previous studies have shown that SUs can reduce input uncertainty more effectively than RUs [54], which is consistent with the findings of this study.

The performance of LR and SLR models differs significantly in areas with high landslide incidence. The LR model predicts a series of high-risk areas in the southwest carbonaceous shale region, the central conglomerate region, and a small portion of the quartz sandstone region. This pattern arises because the LR model heavily relies on lithology factors, causing the predicted high-risk areas to align with lithological trends. However, as shown in Figure 2b, the actual landslide distribution is dispersed, and even within a single lithology area, landslides are not contiguous. This indicates that the LR model, by focusing solely on slope element attributes, erroneously classifies some low-to-medium-risk areas as high-risk. In contrast, the SLR model incorporates not only the attribute

information of mapping units, but also spatial adjacency information, recognizing that the occurrence of landslides in the surrounding units greatly influences the likelihood of landslides within a slope unit. By accounting for these spatial relationships, the SLR model can distinguish three types of risk areas even within a single lithology region. This approach better reflects the heterogeneity of landslide distribution and aligns more closely with real-world conditions.

In general, the prediction accuracy of the SLR model is greatly improved compared with the LR model. The spatial model used in this study incorporates the adjacency information between mapping units. Unlike general regression models, an adjacency matrix aligned with geomorphic characteristics is included, which helps to mitigate the influence of spatial autocorrelation between adjacent units. However, the LR model is a linear model, and the effect is poor when the relationship between landslide and impact factors is not linear and is complicated [43,55]. This enhances the model's precision and the accuracy of landslide susceptibility mapping. However, the SU approach utilized in this paper inherently reduces the impact of spatial autocorrelation on modeling to some extent. To demonstrate more comprehensively the characteristics of the SLR model, it is essential to investigate the influence of the SLR model on spatial autocorrelation under RU and SU unit mapping approaches. This investigation constitutes the next step in our research plan.

GeoDetector's factor detection analysis reveals key differentiation characteristics of landslide susceptibility. Lithology, peak ground velocity (PGV), and distance to the epicenter are identified as the most significant factors, with lithology being the primary determinant of landslide instability. The study area's lithology comprises sand, sandstone, conglomerate, carbonaceous shale, quartz sandstone, and silty rock, accounting for 9%, 6%, 9%, 13%, 51%, and 12% of the slope units, respectively. Although quartz sandstone dominates in area, Figures 3g and 8 show that carbonaceous shale is mainly classified as moderate-to-high-risk, while quartz sandstone is predominantly low-risk. This demonstrates that lithology significantly influences landslide susceptibility. Carbonaceous shale, silty rock, conglomerate, and sandstone are the most landslide-prone lithologies, while soft riverine areas and quartz sandstone are less susceptible. Soft rocks, like sandy loams and carbonaceous shales, deform under seismic vibration, reducing landslide risk by altering their stress state. In contrast, hard rocks such as quartz sandstone resist sliding due to their high shear strength, even during vibrations.

Interaction detection identifies the interplay of multiple factors influencing landslide susceptibility. Figure 9 highlights that the interaction between lithology and peak ground velocity (PGV) exhibits the strongest nonlinear enhancement, followed by the interaction between lithology and distance to the epicenter. Generally, areas with hard lithology are less prone to landslides. However, high-risk zones are observed in some quartz sandstone regions near the focal point (southeast of the study area in Figure 8b). In contrast, in distant focal areas, high-risk zones are more common in regions with soft lithology. This indicates that landslide occurrence is not determined solely by individual factors such as lithology, but by the combined effect of geological conditions and seismic forces. The strong interaction between lithology and PGV suggests that landslides are heavily influenced by the combined effects of seismic dynamics and geological conditions. Similarly, the interaction between lithology and distance to the epicenter underscores the varying impact of geological and dynamic effects at different spatial scales. Specifically, as distance to the epicenter increases, PGV decreases, making soft lithology areas more susceptible to landslides, while hard lithology areas remain less prone. Conversely, closer to the epicenter, even areas with hard lithology exhibit a higher likelihood of landslides due to the amplified seismic effects.

Factor analysis and interaction analysis revealed that geological factors exert a greater influence on landslides than topographic conditions, highlighting earthquakes as the primary triggering factor. Given the challenges posed by topographic conditions, geological factors, wet climates, and the increasing frequency of extreme weather events, greater attention should be paid to the role of geology in landslide occurrence. In landslide

prevention and mitigation, regular geotechnical monitoring is essential [56]. Priority should be given to shale and sandstone areas in slope engineering, where techniques such as shotcrete, bolt support, and other reinforcement methods can be applied to enhance slope shear strength and reduce the likelihood of collapse or landslides. Additionally, using ecological materials such as plant fibers and ecological bags for slope protection not only helps to prevent landslides, but also promotes slope biodiversity, providing both environmental and structural benefits.

The spatial logistic regression (SLR) model incorporates spatial information by considering the connectivity relationships between mapping units. When selecting the spatial adjacency matrix, various methods can be employed, such as the adjacency matrix and the distance matrix. In this study, the connection method used was queen adjacency within the adjacency matrix, which involves connections through common vertices and adjacent edges. Spatial samples based on the queen adjacency rule exhibit a closer correlation with their surrounding spatial units. This adjacency method is straightforward to operate and manage. However, its limitation is that it only considers the influential strength of adjacent units, assigning an influential strength of zero to non-adjacent units. This does not accurately reflect real-world conditions. Therefore, future model improvements should explore different connection methods to achieve a higher prediction accuracy that aligns more closely with actual situations.

6. Conclusions

Landslide susceptibility mapping is of great significance for landslide prediction and control. In this study, slope units were used as the mapping units for landslide susceptibility mapping, ensuring that the results aligned more closely with the actual natural environment. Furthermore, the spatial logistic regression (SLR) model was employed to incorporate the adjacency information of slope units, demonstrating a 26% higher accuracy compared to the logistic regression (LR) model, which does not account for spatial adjacency. This suggests that adjacency information can serve as a valuable new index for landslide susceptibility mapping. Additionally, the driving factors of landslide susceptibility and their interactions were analyzed using GeoDetector. The results identified lithology, peak ground velocity (PGV), and distance to the epicenter as the main factors contributing to landslides. Among these, the interaction between lithology and PGV exhibited the strongest nonlinear enhancement, followed by the interaction between lithology and the epicenter. These findings highlight the importance of considering lithological characteristics and seismic vibration conditions in slope engineering control. By delineating high-risk landslide areas, more precise engineering reinforcement measures and risk warnings can be implemented. This study not only deepens our understanding of the spatial differentiation of landslide susceptibility, but also enhances the practical application of susceptibility mapping in real-world scenarios.

Author Contributions: Conceptualization, J.Y. and L.L.; methodology, J.Y.; validation, M.J.; formal analysis, J.Y. and M.J.; investigation, S.M.; resources, C.X.; data curation, J.Y.; writing—original draft preparation, M.J.; writing—review and editing, L.L., J.Y., Y.T. and M.J.; visualization, M.J.; supervision, L.L.; project administration, L.L.; funding acquisition, L.L. All authors have read and agreed to the published version of the manuscript.

Funding: This research was funded by the National Funding Postdoctoral Fellowship Program of CPSF (GZC20233022); the China Postdoctoral Science Foundation (2024M763573); the Henan Province Fund (232102320002); and the National Institute of Natural Hazards, Ministry of Emergency Management of China (2023-JBKY-57).

Data Availability Statement: The data supporting the findings of this study are available from the corresponding author upon reasonable request.

Acknowledgments: Thanks to Jinfeng Wang, who provided the free-ware GeoDetector, and the contributors of the open-source R package INLA.

Conflicts of Interest: The authors declare no conflicts of interest.

References

1. Petley, D. Global Patterns of Loss of Life from Landslides. *Geology* **2012**, *40*, 927–930. [CrossRef]
2. Youssef, A.M.; Pourghasemi, H.R.; Pourtaghi, Z.S.; Al-Katheeri, M.M. Landslide Susceptibility Mapping Using Random Forest, Boosted Regression Tree, Classification and Regression Tree, and General Linear Models and Comparison of Their Performance at Wadi Tayyah Basin, Asir Region, Saudi Arabia. *Landslides* **2016**, *13*, 839–856. [CrossRef]
3. Fang, K.; Tang, H.; Li, C.; Su, X.; An, P.; Sun, S. Centrifuge Modelling of Landslides and Landslide Hazard Mitigation: A Review. *Geosci. Front.* **2023**, *14*, 101493. [CrossRef]
4. Basharat, M. A Review of Landslides Related to the 2005 Kashmir Earthquake: Implication and Future Challenges. *Nat. Hazards* **2021**, *108*, 1–30. [CrossRef]
5. Huang, Y.; Xu, C.; Zhang, X.; Xue, C.; Wang, S. An Updated Database and Spatial Distribution of Landslides Triggered by the Milin, Tibet Mw6.4 Earthquake of 18 November 2017. *J. Earth Sci.* **2021**, *32*, 1069–1078. [CrossRef]
6. Xu, C.; Xu, X.; Shyu, J.B.H.; Zheng, W.; Min, W. Landslides Triggered by the 22 July 2013 Minxian–Zhangxian, China, Mw 5.9 Earthquake: Inventory Compiling and Spatial Distribution Analysis. *J. Asian Earth Sci.* **2014**, *92*, 125–142. [CrossRef]
7. Chong, X.U. Detailed Inventory of Landslides Triggered by the 2008 Wenchuan Earthquake and Its Comparison with Other Earthquake Events in the World. *Sci. Technol. Rev.* **2012**, *30*, 18–26. [CrossRef]
8. Zhang, S.; Zhang, L.M.; Xiang, B.; Yuan, Q. Travel Distances of Earthquake-Induced Landslides. In Proceedings of the Geo-Congress, San Diego, CA, USA, 25 February 2013; American Society of Civil Engineers: San Diego, CA, USA, 2013; pp. 991–1001.
9. Dai, F.C.; Lee, C.F.; Ngai, Y.Y. Landslide Risk Assessment and Management: An Overview. *Eng. Geol.* **2002**, *64*, 65–87. [CrossRef]
10. Erener, A.; Düzgün, H.S.B. Landslide Susceptibility Assessment: What Are the Effects of Mapping Unit and Mapping Method? *Environ. Earth Sci.* **2012**, *66*, 859–877. [CrossRef]
11. Zhang, T.; Fu, Q.; Quevedo, R.P.; Chen, T.; Luo, D.; Liu, F.; Kong, H. Landslide Susceptibility Mapping Using Novel Hybrid Model Based on Different Mapping Units. *KSCE J. Civ. Eng.* **2022**, *26*, 2888–2900. [CrossRef]
12. Reichenbach, P.; Rossi, M.; Malamud, B.D.; Mihir, M.; Guzzetti, F. A Review of Statistically-Based Landslide Susceptibility Models. *Earth-Sci. Rev.* **2018**, *180*, 60–91. [CrossRef]
13. Yang, J.; Song, C.; Yang, Y.; Xu, C.; Guo, F.; Xie, L. New Method for Landslide Susceptibility Mapping Supported by Spatial Logistic Regression and GeoDetector: A Case Study of Duwen Highway Basin, Sichuan Province, China. *Geomorphology* **2019**, *324*, 62–71. [CrossRef]
14. Arnone, E.; Francipane, A.; Scarbaci, A.; Puglisi, C.; Noto, L.V. Effect of Raster Resolution and Polygon-Conversion Algorithm on Landslide Susceptibility Mapping. *Environ. Model. Softw.* **2016**, *84*, 467–481. [CrossRef]
15. Guzzetti, F.; Galli, M.; Reichenbach, P.; Ardizzone, F.; Cardinali, M. Landslide Hazard Assessment in the Collazzone Area, Umbria, Central Italy. *Nat. Hazards Earth Syst. Sci.* **2006**, *6*, 115–131. [CrossRef]
16. Temme, A.J.A.M.; Heuvelink, G.B.M.; Schoorl, J.M.; Claessens, L. Chapter 5 Geostatistical Simulation and Error Propagation in Geomorphometry. In *Developments in Soil Science*; Elsevier: Amsterdam, The Netherlands, 2009; Volume 33, pp. 121–140. ISBN 978-0-12-374345-9.
17. Huang, F.; Cao, Y.; Li, W.; Catani, F.; Song, G.; Huang, J.; Yu, C. Uncertainties of Landslide Susceptibility Prediction: Influences of Different Study Area Scales and Mapping Unit Scales. *Int. J. Coal Sci. Technol.* **2024**, *11*, 26. [CrossRef]
18. Tanyas, H. A Global Slope Unit-Based Method for the near Real-Time Prediction of Earthquake-Induced Landslides. *Geomorphology* **2019**, *327*, 126–146. [CrossRef]
19. Sun, X.; Chen, J.; Han, X.; Bao, Y.; Zhan, J.; Peng, W. Application of a GIS-Based Slope Unit Method for Landslide Susceptibility Mapping along the Rapidly Uplifting Section of the Upper Jinsha River, South-Western China. *Bull. Eng. Geol. Environ.* **2020**, *79*, 533–549. [CrossRef]
20. Jacobs, L.; Kervyn, M.; Reichenbach, P.; Rossi, M.; Marchesini, I.; Alvioli, M.; Dewitte, O. Regional Susceptibility Assessments with Heterogeneous Landslide Information: Slope Unit- vs. Pixel-Based Approach. *Geomorphology* **2020**, *356*, 107084. [CrossRef]
21. Wang, F.; Xu, P.; Wang, C.; Wang, N.; Jiang, N. Application of a GIS-Based Slope Unit Method for Landslide Susceptibility Mapping along the Longzi River, Southeastern Tibetan Plateau, China. *ISPRS Int. J. Geo-Inf.* **2017**, *6*, 172. [CrossRef]
22. Guzzetti, F.; Carrara, A.; Cardinali, M.; Reichenbach, P. Landslide Hazard Evaluation: A Review of Current Techniques and Their Application in a Multi-Scale Study, Central Italy. *Geomorphology* **1999**, *31*, 181–216. [CrossRef]
23. Luo, W.; Liu, C.-C. Innovative Landslide Susceptibility Mapping Supported by Geomorphon and Geographical Detector Methods. *Landslides* **2018**, *15*, 465–474. [CrossRef]
24. Alvioli, M.; Marchesini, I.; Reichenbach, P.; Rossi, M.; Ardizzone, F.; Fiorucci, F.; Guzzetti, F. Automatic Delineation of Geomorphological Slope Units with r.slopeunits v1.0 and Their Optimization for Landslide Susceptibility Modeling. *Geosci. Model Dev.* **2016**, *9*, 3975–3991. [CrossRef]
25. Wu, H.; Ye, C.; Pei, X.; Oguchi, T.; He, Z.; Yang, H.; Huang, R. Incorporating Effects of Slope Units and Sliding Areas into Seismically Induced Landslide Risk Modeling in Tectonically Active Mountainous Areas. *Remote Sens.* **2024**, *16*, 3517. [CrossRef]
26. Temme, A.; Guzzetti, F.; Samia, J.; Mirus, B.B. The Future of Landslides' Past—A Framework for Assessing Consecutive Landsliding Systems. *Landslides* **2020**, *17*, 1519–1528. [CrossRef]

27. Erener, A.; Düzgün, H.S.B. Improvement of Statistical Landslide Susceptibility Mapping by Using Spatial and Global Regression Methods in the Case of More and Romsdal (Norway). *Landslides* **2010**, *7*, 55–68. [CrossRef]
28. Wu, Z.; Chen, Y.; Han, Y.; Ke, T.; Liu, Y. Identifying the Influencing Factors Controlling the Spatial Variation of Heavy Metals in Suburban Soil Using Spatial Regression Models. *Sci. Total Environ.* **2020**, *717*, 137212. [CrossRef]
29. Jones, J.P.; Foster, S.A. Testing Regression Residuals for Spatial Autocorrelation Using SAS: A Technical Note. *Geogr. Res. Forum* **1991**, *11*, 78–83.
30. Moreiras, S.M. Landslide Susceptibility Zonation in the Rio Mendoza Valley, Argentina. *Geomorphology* **2005**, *66*, 345–357. [CrossRef]
31. Jebur, M.N.; Pradhan, B.; Tehrany, M.S. Optimization of Landslide Conditioning Factors Using Very High-Resolution Airborne Laser Scanning (LiDAR) Data at Catchment Scale. *Remote Sens. Environ.* **2014**, *152*, 150–165. [CrossRef]
32. Chen, T.; Zhu, L.; Niu, R.; Trinder, C.J.; Peng, L.; Lei, T. Mapping Landslide Susceptibility at the Three Gorges Reservoir, China, Using Gradient Boosting Decision Tree, Random Forest and Information Value Models. *J. Mt. Sci.* **2020**, *17*, 670–685. [CrossRef]
33. Guzzetti, F.; Reichenbach, P.; Ardizzone, F.; Cardinali, M.; Galli, M. Estimating the Quality of Landslide Susceptibility Models. *Geomorphology* **2006**, *81*, 166–184. [CrossRef]
34. Tian, Y.; Xu, C.; Hong, H.; Zhou, Q.; Wang, D. Mapping Earthquake-Triggered Landslide Susceptibility by Use of Artificial Neural Network (ANN) Models: An Example of the 2013 Minxian (China) Mw 5.9 Event. *Geomat. Nat. Hazards Risk* **2019**, *10*, 1–25. [CrossRef]
35. Song, Y.; Wang, J.; Ge, Y.; Xu, C. An Optimal Parameters-Based Geographical Detector Model Enhances Geographic Characteristics of Explanatory Variables for Spatial Heterogeneity Analysis: Cases with Different Types of Spatial Data. *GIScience Remote Sens.* **2020**, *57*, 593–610. [CrossRef]
36. Yang, J.; Xu, C.; Jin, X. Joint Effects and Spatiotemporal Characteristics of the Driving Factors of Landslides in Earthquake Areas. *J. Earth Sci.* **2023**, *34*, 330–338. [CrossRef]
37. Tian, Y.; Xu, C.; Xu, X.; Chen, J. Detailed Inventory Mapping and Spatial Analyses to Landslides Induced by the 2013 Ms 6.6 Minxian Earthquake of China. *J. Earth Sci.* **2016**, *27*, 1016–1026. [CrossRef]
38. Ma, S.; Shao, X.; Xu, C. Landslide Susceptibility Mapping in Terms of the Slope-Unit or Raster-Unit, Which Is Better? *J. Earth Sci.* **2023**, *34*, 386–397. [CrossRef]
39. García, D.; Mah, R.T.; Johnson, K.L.; Hearne, M.G.; Marano, K.D.; Wald, D.J.; Worden, C.B. ShakeMap Atlas 2.0: An Improved Suite of Recent Historical Earthquake ShakeMaps for Global Hazard Analyses and Loss Model Calibration. In Proceedings of the World Conference on Earthquake Engineering 2012, Lisbon, Portugal, 24–28 September 2012.
40. Schlögel, R.; Marchesini, I.; Alvioli, M.; Reichenbach, P.; Rossi, M.; Malet, J.-P. Optimizing Landslide Susceptibility Zonation: Effects of DEM Spatial Resolution and Slope Unit Delineation on Logistic Regression Models. *Geomorphology* **2018**, *301*, 10–20. [CrossRef]
41. Chalkias, C.; Kalogirou, S.; Ferentinou, M. Landslide Susceptibility, Peloponnese Peninsula in South Greece. *J. Maps* **2014**, *10*, 211–222. [CrossRef]
42. Gamerman, D.; Moreira, A.R.B. Multivariate Spatial Regression Models. *J. Multivar. Anal.* **2004**, *91*, 262–281. [CrossRef]
43. Cao, J.; Zhang, Z.; Wang, C.; Liu, J.; Zhang, L. Susceptibility Assessment of Landslides Triggered by Earthquakes in the Western Sichuan Plateau. *CATENA* **2019**, *175*, 63–76. [CrossRef]
44. Bakka, H.; Rue, H.; Fuglstad, G.-A.; Riebler, A.; Bolin, D.; Illian, J.; Krainski, E.; Simpson, D.; Lindgren, F. Spatial Modeling with R-INLA: A Review. *WIREs Comput. Stat.* **2018**, *10*, e1443. [CrossRef]
45. Lombardo, L.; Opitz, T.; Huser, R. Numerical Recipes for Landslide Spatial Prediction Using R-INLA. In *Spatial Modeling in GIS and R for Earth and Environmental Sciences*; Elsevier: Amsterdam, The Netherlands, 2019; pp. 55–83. ISBN 978-0-12-815226-3.
46. Wang, J.-F.; Zhang, T.-L.; Fu, B.-J. A Measure of Spatial Stratified Heterogeneity. *Ecol. Indic.* **2016**, *67*, 250–256. [CrossRef]
47. Wang, J.; Li, X.; Christakos, G.; Liao, Y.; Zhang, T.; Gu, X.; Zheng, X. Geographical Detectors-Based Health Risk Assessment and Its Application in the Neural Tube Defects Study of the Heshun Region, China. *Int. J. Geogr. Inf. Sci.* **2010**, *24*, 107–127. [CrossRef]
48. Wang, J.-F.; Hu, Y. Environmental Health Risk Detection with GeogDetector. *Environ. Model. Softw.* **2012**, *33*, 114–115. [CrossRef]
49. Beguería, S. Validation and Evaluation of Predictive Models in Hazard Assessment and Risk Management. *Nat. Hazards* **2006**, *37*, 315–329. [CrossRef]
50. Cantarino, I.; Carrion, M.A.; Goerlich, F.; Martinez Ibañez, V. A ROC Analysis-Based Classification Method for Landslide Susceptibility Maps. *Landslides* **2019**, *16*, 265–282. [CrossRef]
51. Yilmaz, C.; Topal, T.; Süzen, M.L. GIS-Based Landslide Susceptibility Mapping Using Bivariate Statistical Analysis in Devrek (Zonguldak-Turkey). *Environ. Earth Sci.* **2012**, *65*, 2161–2178. [CrossRef]
52. Pourghasemi, H.R.; Moradi, H.R.; Fatemi Aghda, S.M. Landslide Susceptibility Mapping by Binary Logistic Regression, Analytical Hierarchy Process, and Statistical Index Models and Assessment of Their Performances. *Nat. Hazards* **2013**, *69*, 749–779. [CrossRef]
53. Zhou, X.; Wen, H.; Zhang, Y.; Xu, J.; Zhang, W. Landslide Susceptibility Mapping Using Hybrid Random Forest with GeoDetector and RFE for Factor Optimization. *Geosci. Front.* **2021**, *12*, 101211. [CrossRef]
54. Bornaetxea, T.; Rossi, M.; Marchesini, I.; Alvioli, M. Effective Surveyed Area and Its Role in Statistical Landslide Susceptibility Assessments. *Nat. Hazards Earth Syst. Sci.* **2018**, *18*, 2455–2469. [CrossRef]

55. Shao, X.; Ma, S.; Xu, C.; Zhang, P.; Wen, B.; Tian, Y.; Zhou, Q.; Cui, Y. Planet Image-Based Inventorying and Machine Learning-Based Susceptibility Mapping for the Landslides Triggered by the 2018 Mw6.6 Tomakomai, Japan Earthquake. *Remote Sens.* **2019**, *11*, 978. [CrossRef]
56. Confuorto, P.; Di Martire, D.; Infante, D.; Novellino, A.; Papa, R.; Calcaterra, D.; Ramondini, M. Monitoring of Remedial Works Performance on Landslide-Affected Areas through Ground- and Satellite-Based Techniques. *CATENA* **2019**, *178*, 77–89. [CrossRef]

Disclaimer/Publisher's Note: The statements, opinions and data contained in all publications are solely those of the individual author(s) and contributor(s) and not of MDPI and/or the editor(s). MDPI and/or the editor(s) disclaim responsibility for any injury to people or property resulting from any ideas, methods, instructions or products referred to in the content.